Protegrin interaction with lipid monolayers: grazing incidence X-ray diffraction and X-ray reflectivity study†

Frances Neville,‡[a] Yuji Ishitsuka,§[b] Chris S. Hodges,[a] Oleg Konovalov,[c] Alan J. Waring,[c] Robert Lehrer,[d] Ka Yee C. Lee[b] and David Gidalevitz*[e]

Received 28th November 2007, Accepted 30th April 2008
First published as an Advance Article on the web 19th June 2008
DOI: 10.1039/b718295c

Interactions of the antimicrobial peptide protegrin-1 (PG-1) with phospholipid monolayers have been investigated by using grazing incidence X-ray diffraction (GIXD) and specular X-ray reflectivity (XR). The structure of a PG-1 film at the air–aqueous interface was also investigated by XR for the first time. Dipalmitoyl phosphatidylcholine (DPPC), dipalmitoyl phosphatidylglycerol (DPPG) and lipid A monolayers were formed at the air–aqueous interface to mimic the surface of human erythrocytes, Gram-positive bacterial cell membranes and Gram-negative bacterial outer membranes, respectively. Experiments were carried out under constant area conditions where the pressure changes upon insertion of peptide into the monolayer. GIXD data suggest that the greatest monolayer disruption produced by PG-1 is seen with the DPPG system at 20 mN m^{-1} since the Bragg peaks completely disappear after introduction of PG-1 to the system. PG-1 shows greater insertion into the lipid A system compared to the DPPC system when both films are held at the same initial surface pressure of 20 mN m^{-1}. The degree of insertion lessens at 30 mN m^{-1} with both DPPC and DPPG monolayer systems. XR data further reveal that PG-1 inserts primarily in the head group region of lipid monolayers. However, only the XR data of the anionic lipids suggest the existence of an additional adsorbed peptide layer below the head group of the monolayer. Overall, the data show that the extent of peptide–lipid interaction and lipid monolayer disruption depends not only on the lipid composition of the monolayer, but the packing density of the lipids in the monolayer prior to the introduction of peptide to the subphase.

Introduction

The last decade has seen a considerable increase in the study of antimicrobial peptides due to the interest for their potential as future pharmaceutical drug compounds.[1] Antimicrobial peptides have a broad spectrum of antimicrobial properties and serve as inducers and modulators of various chemical components of the innate immune system.[2]

Recent work has shown that antimicrobial peptides act by permeating cell membranes.[3,4] Although it is evident that the cell membrane is a barrier that must be overcome by antimicrobial peptides for cell disruption, the exact mechanism of action of antimicrobial peptides remains unclear.[5] It has been established that antimicrobial peptides have the ability to differentiate between foreign and native cells,[4,6–8] and one of the main reasons for this is thought to be due to the different lipid components and physical properties of the cell membranes involved.

Eukaryotic and bacterial membranes have very different lipid compositions. The mammalian cell membrane consists mainly of phosphatidylcholine (PC), phosphatidylethanolamine (PE), sphingomyelin, and cholesterol,[6,9] with the outer leaflet being enriched in PC.[5,10] This is vastly different from bacterial membranes, which contain a high proportion of negatively charged lipids such as phosphatidylglycerol (PG) and PG derivatives such as diphosphatidylglycerol or cardiolipin.[5,6] The lipid components of bacterial membranes also depend on the classification of the bacterium into Gram-positive or Gram-negative classes.[11] Gram-positive bacteria such as *Staphylococcus aureus* have a single membrane that contains a high level of PG lipids, whereas Gram-negative bacteria have, in addition to the plasma membrane, an outer cell wall coated with lipopolysaccharide (LPS), of which lipid A acts as the lipophilic anchor.[12] Since lipid A is an important component of the outer membrane of Gram-negative bacteria, it is a prospective target for the design of novel antibacterial drug compounds.

[a]*School of Process, Environmental and Materials Engineering, University of Leeds, Leeds, LS2 9JT, UK*
[b]*Department of Chemistry, The Institute for Biophysical Dynamics and the James Franck Institute, The University of Chicago, Chicago, Illinois 60637, USA*
[c]*European Synchrotron Radiation Facility, 6 Rue Jules Horowitz, BP 220, F-38043 Grenoble Cedex, France*
[d]*Department of Medicine, University of California at Los Angeles School of Medicine, Los Angeles, California 90095, USA*
[e]*Division of Physics and Center for Synchrotron Radiation Research and Instrumentation, BCPS Department, Illinois Institute of Technology, Chicago, Illinois 60616, USA; Fax: +1 312 567 8874; Tel: +1 312 567 3534*
† Electronic supplementary information (ESI) available: 1. Example of Bragg rod and Bragg peak profiles; 2. Comparison of L_1 XR fitting values and those obtained from tilt angles. See DOI: 10.1039/b718295c
‡ *Present address*: Institute of Membrane and Systems Biology, University of Leeds, Leeds, LS2 9JT, UK. Email: F.C.Neville@leeds.ac.uk; Tel: +44 113 343 1435.
§ *Present address*: Howard Hughes Medical Institute and Department of Physics, University of Illinois Urbana-Champaign, Urbana, Illinois 61801-308, USA.

In this paper the interactions of an antimicrobial peptide, protegrin-1 (PG-1¶), with DPPC¶, DPPG¶ and lipid A monolayers are examined under constant area conditions. These lipids are present in the outer leaflet of human erythrocytes, Gram-positive bacterial cell membranes and Gram-negative bacterial outer membranes, respectively.

Protegrin-1 is an arginine- and cysteine-rich antimicrobial peptide, originally isolated from porcine leukocytes.[13,14] It contains 18 amino acid residues and a net charge of +6 due to six arginine residues. NMR studies show that it has a one-turn β-hairpin structure that includes two disulfide bonds when in solution.[15] Members of the protegrin family have been shown to exhibit anti-human immunodeficiency virus type-1 activity *in vitro*[16] and activity against *Chlamydiae*,[17] among other antimicrobial properties.

Previous work[18] using oriented circular dichroism has studied the alignment of PG-1 in lipid bilayers. It has been proposed that the PG-1 peptide exists in membranes in two different states, which correspond to the surface adsorbed state and the inserted state, similar to that of the α-helical antimicrobial peptide, alamethicin.[18] In the surface state, PG-1 is adsorbed to the head group region of a lipid bilayer with the peptide being oriented parallel to bilayer, whereas in the inserted state, the peptide is orientated perpendicular to the lipid bilayer plane. Ma *et al.*[19] observed a PG-1 induced thickness change and a kinetic profile that corroborates with this model by using surface plasmon resonance.

More recently, Mani *et al.*[20,21] used solid-state NMR to investigate the oligomeric structure and insertion of PG-1 into lipid bilayers. Their studies on the dimeric structure of PG-1 molecules in palmitoyloleoylphosphatidylcholine (POPC) bilayers suggest that two PG-1 molecules align in a parallel fashion.[20] Further work was carried out with lipids that mimic the bacterial inner membrane or the red blood cell membrane. The results of Mani *et al.* suggest that PG-1 adopts dramatically different oligomeric structures depending on the lipid composition of the membrane with much greater contact of the peptide with anionic lipids than with those that mimic the red blood cell membrane (POPC/cholesterol).[21]

The interactions of PG-1 with various lipid monolayers have also been recently studied to model the initial interaction of PG-1 with the outer leaflet of the cell membrane.[22,23] Different lipid compositions were used to represent the membrane of various cell types, and these systems were studied by insertion assay, epifluorescence microscopy and X-ray scattering techniques under constant pressure and constant area conditions. These studies showed that PG-1 readily inserts into lipid monolayers of phosphatidylglycerol lipids and lipid A, but significantly less so into lipid monolayers of phosphatidylcholine lipids.[22,23]

In this paper, the interaction of PG-1 with lipid monolayers was carried out by monitoring insertion under constant area conditions where changes in surface pressure indicate the degree of interaction of peptide with the lipid layer. This paper not only consolidates and reinforces earlier work carried out using epifluorescence microscopy and X-ray scattering methods[22,23] but it also presents a thorough investigation of the interaction of PG-1 with different lipids, which has not been published to date. Moreover, the importance of the effect of the initial surface pressure, and hence lipid packing density, of the different monolayers on subsequent peptide-induced disorder is discussed.

¶ Abbreviations: DPPC = dipalmitoyl phosphatidylcholine; DPPG = dipalmitoyl phosphatidylglycerol; GIXD = grazing incidence X-ray diffraction; XR = X-ray reflectivity; PG 1 = protegrin-1.

Results

Generally, there are two different ways to conduct peptide-injection experiments: constant pressure and constant area conditions. At constant pressure conditions the pressure is fixed at particular value (here 20 mN m^{-1}), and if peptides insert into the monolayer, the trough barrier relaxes in order to allow peptides to incorporate into the lipid monolayer. Any change in the area occupied by the monolayer following injection can be translated into a relative change in the lipid area per molecule ($\Delta A/A$). With constant area injection experiments, the barrier is not allowed to move, therefore, if peptide insertion occurs the surface pressure has to increase, because more molecules occupy the same area. In this case, a relative pressure change ($\Delta P/P$) upon injection gives indication of surface activity of particular peptide. All experiments discussed in this paper were conducted under constant area conditions.

GIXD – systems at 20 mN m^{-1}

GIXD measurements of lipid monolayers before and after injection of PG-1 were carried out for DPPC, DPPG and lipid A monolayers under constant area conditions after compression to 20 mN m^{-1}. GIXD data of these systems are shown in Fig. 1. The top and the bottom scans correspond to the GIXD scan after and before the injection of PG-1, respectively. The corresponding values of unit-cell dimensions, *d*-spacings, correlation length and tilt angle can be found in Table 1. In all cases, two Bragg peaks indicate the presence of an ordered structure with centered rectangular packing for pure lipid monolayers. The correlation length gives a measure of length restriction caused by inhomogeneities in the sample, and a reduction in the correlation length is indicative that the monolayer has more impurities or it is made of two components, such as the monolayer and peptide inserting in to the monolayer. The tilt angle gives an idea of the tail group order and can be used to corroborate values obtained with XR layer fitting.

The data for the DPPC systems after PG-1 injection under constant area conditions (Fig. 1a) show a decrease in peak intensity and a shift in the peak positions. The insertion of PG-1 into this system gave an increase in surface pressure of 12 mN m^{-1} over the time scale of 20 minutes, corroborating the shift in the positions of the Bragg peaks observed in Fig. 1a, signifying that the area per molecule decreases on peptide injection due to lipid compression. This is also corroborated by a decrease in correlation length, suggesting that the DPPC monolayer becomes more inhomogeneous after peptide insertion.

The effect of PG-1 insertion on DPPG monolayers at 20 mN m^{-1} (Fig. 1b) is very different from that of the DPPC system after PG-1 insertion. Here the previously ordered structure, shown by the two Bragg peaks, completely disappears (Fig. 1b). The pressure increased on insertion of PG-1 under the DPPG

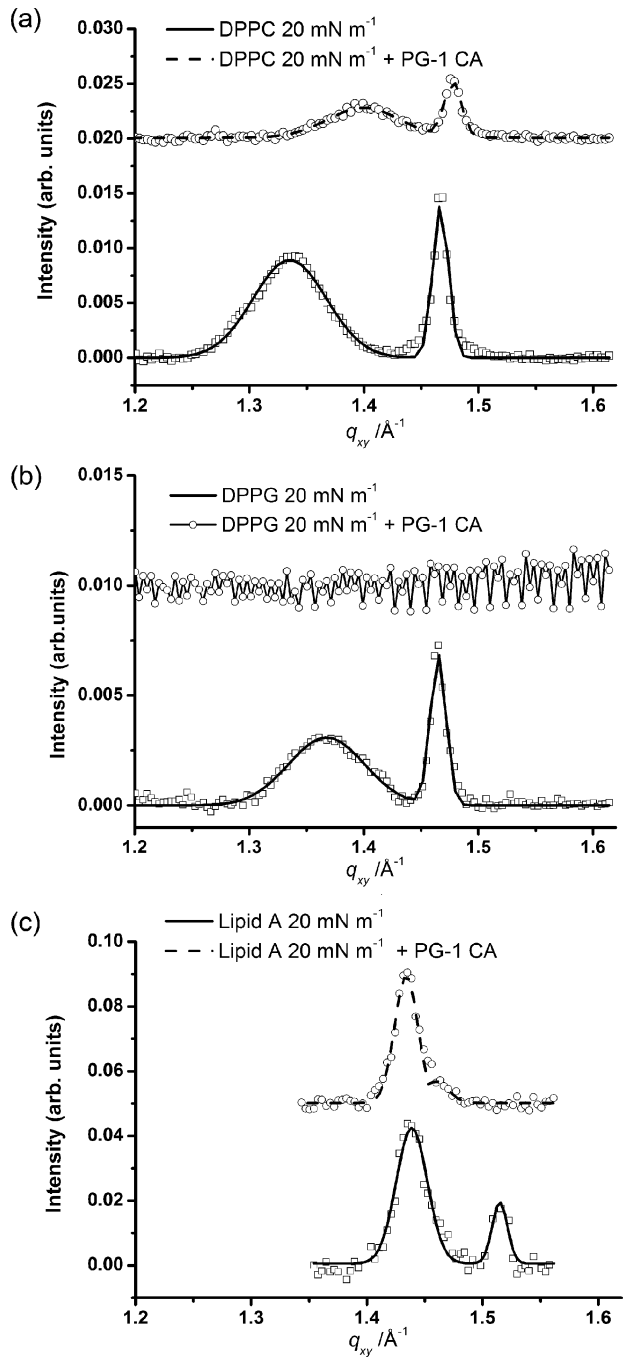

Fig. 1 Bragg peak plot of scattering vector q_{xy} as a function of intensity – monolayers at 20 mN m^{-1}. (a) Data (□) and fit (—) of DPPC monolayer at 20 mN m^{-1}; data (○) and fit (—) of DPPC monolayer after 0.025 mg ml^{-1} PG-1 injection into the subphase. (b) Data (□) and fit (—) of DPPG monolayer at 20 mN m^{-1}; data (-○-) of DPPG monolayer at 20 mN m^{-1} after 0.025 mg ml^{-1} PG-1 injection into the subphase. C) Data (□) and fit (—) of lipid A monolayer at 20 mN m^{-1} (—); data (○) and fit (—) of lipid A monolayer after 0.025 mg ml^{-1} PG-1 injection into the subphase. For clarity the data have been offset vertically.

monolayer and was 28.7 mN m^{-1}, 25 minutes after peptide injection.

GIXD data for the pure lipid A monolayer at an initial surface pressure of 20 mN m^{-1} are compared with data for lipid A system after the injection of PG-1 (Fig. 1c). The *d*-spacings and unit-cell dimensions calculated for lipid A before and after PG-1 injection have been performed based on the assumption that the molecule contains six acyl chains on average, as determined previously.[31] Unlike DPPG, the lipid A monolayer remains crystalline after introduction of PG-1, although the area per lipid A molecule has apparently grown. This apparent increase in area per lipid A molecule seems to be due to the effect of an increase in intermolecular lipid A spacing (seen from the negative shift of the {02} peak, most likely due to PG-1 penetration) rather than the intramolecular spacing (spacing between lipid A tails, {11} peak), which is very similar before and after peptide injection. There was also an increase in pressure upon insertion of peptide of 19 mN m^{-1}, which strongly suggests that peptide penetration occurred and forced the lipid A molecules apart, whilst the conformation of the individual lipid A molecules remained the same.

GIXD – 30 mN m^{-1} systems

The GIXD data for the DPPC system at 30 mN m^{-1} before and after injection of PG-1 are shown in Fig. 2a. The data after injection of PG-1 show that the area per molecule remains roughly the same as the pure DPPC monolayer at 30 mN m^{-1} (Table 1). This suggests that the higher pressure of 30 mN m^{-1} and constant area conditions hinder peptide incorporation into the monolayer.

The PG-1 peptide imparts a smaller degree of disordering on the DPPG monolayer at 30 mN m^{-1} (Fig. 2b) compared to that at 20 mN m^{-1} (Fig. 1b). The peak intensities decrease upon PG-1 injection, suggesting that the area fraction of the ordered phase has diminished due to the presence of the peptide. However, unlike at the lower surface pressure, two Bragg peaks can still be observed even in the presence of the peptide.

XR – PG-1 at the air–aqueous interface

To assess the surface adsorption of the peptide, a study of PG-1 itself at the air–aqueous interface was carried out. The peptide was injected into the subphase of the trough under constant area conditions in the absence of a lipid monolayer (initial surface pressure was 0 mN m^{-1}). Upon injection of PG-1 into the subphase, the surface pressure increased from 0 to 17 mN m^{-1}, suggesting the formation of a PG-1 film at the air–aqueous interface. XR measurements were then carried out on this PG-1 film after the surface pressure reached equilibrium. Fig. 3 shows the XR data and the corresponding fit obtained from the analysis of the data. The data were fitted and a two-layer model was needed to adequately fit the data. The fitting returned values of layer thickness of 12.2 and 12.7 Å for L_1 and L_2, respectively, with the layer nearest the air, termed L_1, and the layer nearest to the subphase, termed L_2. The respective electron densities for these layers normalized to the electron density of the subphase (0.337 e$^-$ Å^{-3}) were 1.45 and 1.05. This electron density profile suggests the formation of peptide bilayer at the air–aqueous interface.

XR – interactions of PG-1 with lipid monolayers at 20 mN m^{-1}

The reflectivity curves (normalized to the Fresnel reflectivity of a planar interface) for the DPPC and lipid A monolayers at

Table 1 Grazing incidence X-ray diffraction data of lipid systems before and after injection of PG-1 under constant area conditions

Experiment	D_{11}[a]/Å	d_{02}[a]/Å	a/Å	b/Å	Area per molecule/Å^2	Correlation length/Å		Tilt/°
						L_{11}[a]	L_{02}[a]	
DPPC 20 mN m^{-1}	4.71	4.28	5.63	8.57	48.3	~85	~542	49
DPPC 20 mN m^{-1} + PG-1	4.49	4.25	5.29	8.5	44.9	~91	~498	29
DPPG 20 mN m^{-1}	4.59	4.29	5.44	8.58	46.7	~91	~593	33
DPPG 20 mN m^{-1} + PG-1	—	—	—	No peaks	—	—	—	—
Lipid A 20 mN m^{-1}	4.34	4.15	5.09	8.3	126.9	~220	~550	N/A
Lipid A 20 mN m^{-1} + PG-1	4.38	4.3	5.09	8.61	131.4	~316	~296	N/A
DPPC 30 mN m^{-1}	4.60	4.26	5.47	8.53	46.6	~126	~1062	30
DPPC 30 mN m^{-1} + PG-1	4.61	4.28	5.47	8.56	46.8	~109	~518	30
DPPG 30 mN m^{-1}	4.51	4.25	5.32	8.51	45.2	~75	~448	27
DPPG 30 mN m^{-1} + PG-1	4.60	4.28	5.46	8.56	46.7	~71	~192	32

[a] "11" and "02" are used to denote (hk) for a set of Bragg rods with equal in-plane components that cannot be resolved from the GIXD data. In this case, data are calculated using the rectangular unit cell, thus {11} lattice means {(11), (1$\bar{1}$), ($\bar{1}$1), ($\bar{1}$ $\bar{1}$)} and {02} means {(02), (0 $\bar{2}$)}.

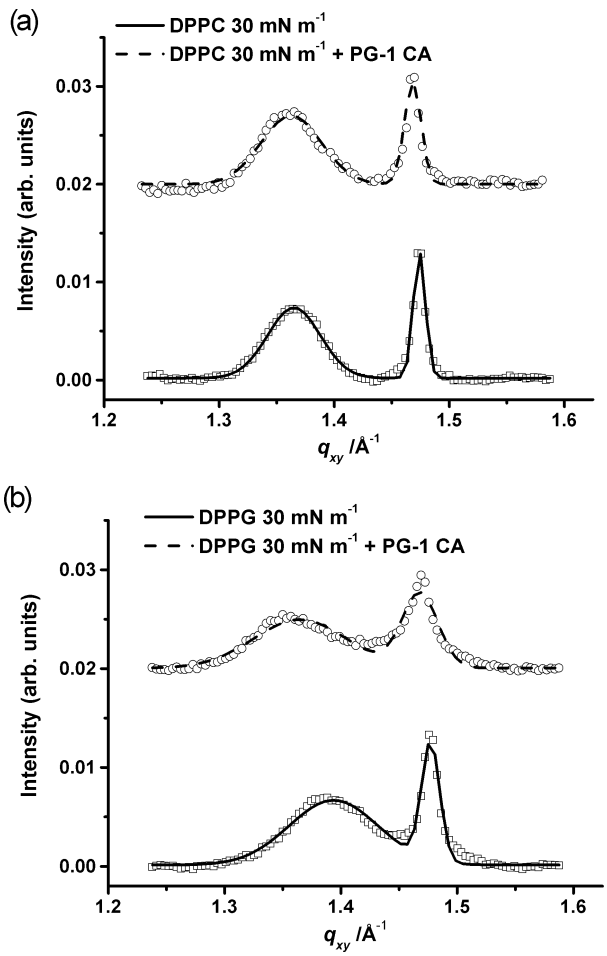

Fig. 2 Bragg peak plot of scattering vector q_{xy} as a function of intensity – monolayers at 30 mN m^{-1}. A) Data (□) and fit (—) of DPPC monolayer at 30 mN m^{-1}; data (○) and fit (—) of DPPC monolayer after 0.025 mg ml^{-1} PG-1 injection into the subphase; B) Data (□) and fit (—) of DPPG monolayer at 30 mN m^{-1} (—); data (○) and fit (—) of DPPG monolayer at 30 mN m^{-1} after 0.025 mg ml^{-1} PG-1 injection into the subphase. For clarity the data have been offset vertically.

20 mN m^{-1} before and after injection of PG-1 into the subphase are shown in Fig. 4. Corresponding fit parameters are shown in Table 2.

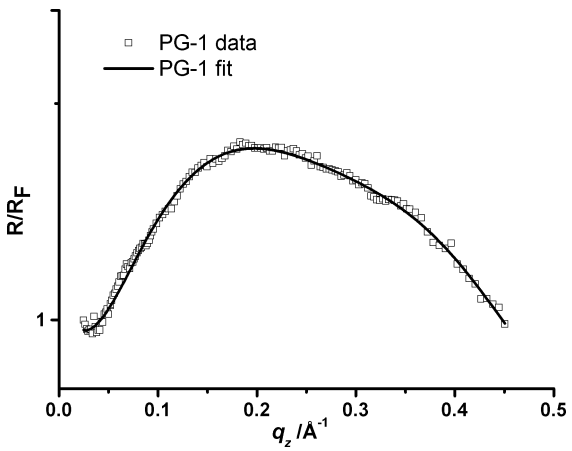

Fig. 3 X-Ray reflectivity data and corresponding fits normalized by Fresnel reflectivity plotted against scattering vector (q_z) of PG-1 at air–aqueous interface at 17 mN m^{-1}. PG-1 reflectivity data (□) and fit (—). For clarity the data have been offset vertically.

For pure lipid monolayers, the L_1 layer corresponds to the tail group region of the phospholipid, and the L_2 layer the head group region. The tilt value for the pure DPPC monolayer at 20 mN m^{-1} was 49°, which corresponds to a tail length (L_1) of 12.6Å, which is the same value as that obtained with the XR fitting. Other values of tilt (Table 1) corresponded to similar values of those obtained with the XR fitting and all were within the limits of the roughness values obtained (see ESI†).

After injection of PG-1 under the DPPC monolayer at 20 mN m^{-1} (Fig. 4a), the layer thicknesses remain similar, but the normalized electron densities increase and decrease for the L_1 and L_2 layers, respectively (Table 2). The corresponding GIXD data suggest that there is insertion of some peptide into the film as a decrease in intensity of the Bragg peaks was observed. Put together, the XR and GIXD data indicate that the insertion is mainly into the head group region, perhaps with some minor partitioning of PG-1 into the base of the tail group region.

XR data of the pure lipid A monolayer at 20 mN m^{-1} were compared with those of the same lipid film at 20 mN m^{-1} but after PG-1 injection into the subphase (Fig. 4b). The lipid A with PG-1 system was modeled with three slabs and the results are listed in Table 2. An additional slab had to be added in order to

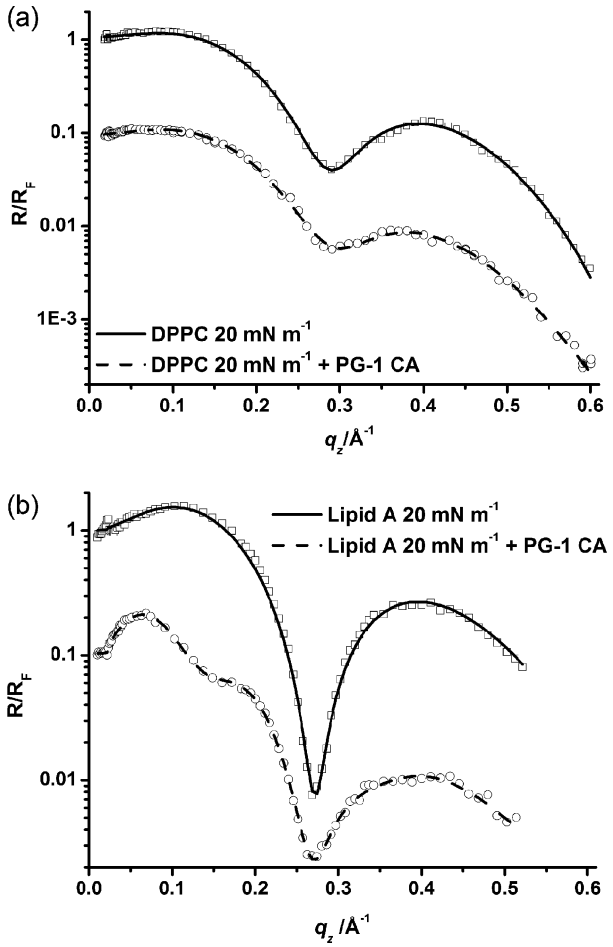

Fig. 4 X-Ray reflectivity data and corresponding fits normalized by Fresnel reflectivity plotted against scattering vector (q_z) of lipid monolayers at 20 mN m^{-1}. (a) DPPC at 20 mN m^{-1} reflectivity data (□) and fit (—); DPPC + 0.025 mg ml^{-1} PG-1 (at 20 mN m^{-1} constant area conditions), data (○) and fit (—). (b) lipid A at 20 mN m^{-1} reflectivity data (□) and fit (—); lipid A + 0.025 mg ml^{-1} PG-1 (at 20 mN m^{-1} constant area conditions), data (○) and fit (—). For clarity the data have been offset vertically.

model the system adequately. The slab nearest the air was named L_1, the next slab L_2, and the slab closest to the subphase, L_3. The increase in electron density of L_1 along with the decrease of electron density of L_2 indicates that the PG-1 molecules have fully inserted into the lipid A monolayer. This is expected since the electron densities of the pure peptide layers are known to be higher and lower than the lipid tail and head group layers, respectively. The third layer, L_3, is 26.6 Å thick with a normalized electron density of 1.22. This suggests that the peptide may insert and hang down perpendicular to the monolayer or that multilayers may adsorb underneath the lipid monolayer.

For reasons of comparison and completeness, the fitting results for the DPPG at 20 mN m^{-1} system before and after injection of PG-1 as previously published[22] are presented in Table 2. It is interesting to note that the results from the data fitting for the DPPG and lipid A systems after PG-1 injection are quite similar with regards to layer thicknesses. Especially noteworthy is the fact that both anionic lipid systems require a third layer to be modeled, which is of a similar thickness (~27 Å). It turns out that this value is approximately the known length of the PG-1 molecule,[22,25] suggesting that at 20 mN m^{-1} the PG-1 peptide most likely orients with its long axis almost perpendicular to the interface or forms multi-adlayers in both the lipid A and DPPG systems.

XR – interactions of PG-1 with lipid monolayers at 30 mN m^{-1}

Fig. 5a shows the normalized reflectivity curves for the DPPC system at 30 mN m^{-1} before and after injection of PG-1 under constant area conditions. The fitted parameters for the DPPC monolayer at 30 mN m^{-1} can be seen in Table 2. After injection of PG-1, the data could again be fitted with two layers. The data suggest that the PG-1 peptides penetrate into the head group layer (as shown by the decrease in electron density and the increase in thickness of the head group layer).

Fig. 5b shows the comparison of the X-ray reflectivity data for the DPPG system at 30 mN m^{-1} before and after injection of PG-1 under constant area conditions. The data suggest that the head group region was again targeted, as was the case with DPPC under the same experimental conditions. The data for the DPPG with PG-1 system had to be modeled using three layers (Table 2). However, the third layer did not have the same

Table 2 X-Ray reflectivity data of lipid systems before and after injection of PG-1 under constant area conditions[a]

Experiment	L_1/Å[a]	ρ_1[a]	L_2/Å[a]	ρ_2[a]	L_3/Å	ρ_3[a]	Roughness$_{L_1}$ σ/Å
DPPC at 20 mN m^{-1}	12.6	0.9	7.1	1.25	—	—	4.0
DPPC 20 mN m^{-1} + PG-1	12.5	0.97	8.5	1.19	—	—	4.2
Lipid A 20 mN m^{-1}	13.3	0.99	5.1	1.65	—	—	4.0
Lipid A 20 mN m^{-1} + PG-1	12.3	1.04	8.8	1.37	26.6	1.22	4.6
DPPG at 20 mN m−1[22]	12.3	0.92	8.4	1.30	—	—	N/A
DPPG 20 mN m^{-1} + PG-1[22]	13.9	1.22	7.0	1.27	27.2	1.07	N/A
DPPC at mN m^{-1}	15.2	0.91	8.8	1.33	—	—	3.3
DPPC 30 mN m^{-1} + PG-1	16.1	0.96	11.6	1.12	—	—	5.5
DPPG at 30 mN m^{-1}	18.1	0.98	5.9	1.55	—	—	3.7
DPPG 30 mN m^{-1} + PG-1	14.9	0.98	6.9	1.39	6.1	1.21	5.2

[a] L_1 refers to the slab closest to the air and the subsequent slabs (L_{2-4}) proceed in order from the slab next nearest to the air to the slab nearest the aqueous subphase. ρ_n is the electron densities of these layers, where n is the corresponding layer number. The reported electron densities are normalized by the electron density value of the DPBS subphase (0.337 e$^-$ Å^{-3}). Data shows comparison of systems before and after addition of PG-1 to the different lipid systems.

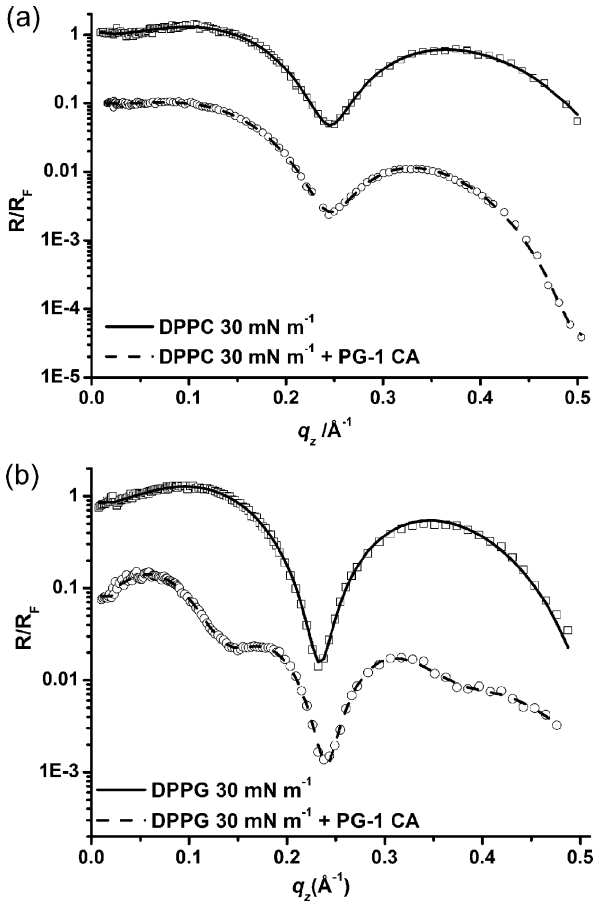

Fig. 5 X-Ray reflectivity data and corresponding fits normalized by Fresnel reflectivity plotted against scattering vector (q_z) of DPPC and DPPG monolayers at 30 mN m^{-1}. (a) DPPC at 30 mN m^{-1} reflectivity data (□) and fit (—); DPPC + 0.025 mg ml^{-1} PG-1, data (○) and fit (—); (b) DPPG at 30 mN m^{-1} reflectivity data (□) and fit (—); DPPG + 0.025 mg ml^{-1} PG-1, data (○) and fit (—). For clarity the data have been offset vertically.

thickness as the third layer for the lipid A and DPPG systems with PG-1 at 20 mN m^{-1}, suggesting that an adsorbed layer of peptide oriented perpendicular to the interface is not present at 30 mN m^{-1}, and that it is more likely that the third layer is made up of peptide that has not fully inserted into the monolayer but rather with portions of it sticking out into the subphase.

Discussion

GIXD – 20 mN m^{-1} systems

Data from the DPPC with PG-1 system show that the calculated area per molecule value decreases slightly from the value of the pure DPPC monolayer at 20 mN m^{-1} (Fig. 1a). This is thought to be due to the monolayer being forced to pack more tightly upon peptide insertion under the constant area conditions since the surface area of the trough being used is kept constant. Comparing this case with that at 30 mN m^{-1}, lipids at 20 mN m^{-1} have a lower packing density, and should have greater lipid mobility and hence allow greater ease for peptide insertion compared to the 30 mN m^{-1} DPPC system. Indeed, this is confirmed by our GIXD data where the DPPC system at 20 mN m^{-1} changes much more noticeably after PG-1 insertion (Fig. 1a) than the DPPC system at 30 mN m^{-1} after PG-1 injection (Fig. 2a). This is further confirmed by the fact that no discernible pressure change was observed for the 30 mN m^{-1} DPPC system after peptide injection.

GIXD data for the DPPG with PG-1 system at 20 mN m^{-1} indicate that the DPPG monolayer becomes completely disordered upon insertion of PG-1 even on the Ångstrom scale. This and the fact that there is a 44 % increase in surface pressure corroborates our earlier findings of micron-scale domains originally observed *via* epifluorescence microscopy in a DPPG monolayer disappearing upon the introduction of PG-1 into the subphase.[22,23]

The lipid A data suggest that under constant area conditions the individual "tails" of each lipid A molecule remain with a similar conformation before and after injection of PG-1, and that the inferred peptide insertion based on the observation of an increased pressure is due to peptide penetration into the lipid A monolayer, mostly in the head group regions. Since the structure of the tail region of the lipid A molecule seems to be rigid,[31] it is reasonable to assume that the insertion occurs mostly in the head group regions. The data also show that the {11} peak is largely unaffected, but that the {02} peak decreases in size and is significantly shifted to a lower q_{xy} value by around 0.05 Å^{-1}. Since the lipid A molecule has six hydrocarbon chains on average,[31] the {11} peak corresponds to intramolecular tail–tail distances, while the {02} peak corresponds to intermolecular lipid A – lipid A molecule distances. Upon PG-1 insertion into the lipid A head group region, the area per lipid molecule increases, and the intermolecular distance increases correspondingly, as signified by a shift of the {02} peak to a lower q_{xy} region. In other words, the data suggest that the apparent area per lipid A molecule is increasing as the PG-1 is inserting in between lipid A molecules.

GIXD – 30 mN m^{-1} systems

GIXD data for the DPPC systems at 30 mN m^{-1} (Fig. 2a) show some differences from those for DPPC at 20 mN m^{-1} (Fig. 1a). The DPPC monolayer at 30 mN m^{-1} (Fig. 2a) again shows an ordered structure, giving rise to Bragg peaks just as in the case at 20 mN m^{-1} (Fig. 1a). However, unlike at 20 mN m^{-1}, upon injection of PG-1 at 30 mN m^{-1}, there is very little change in both the peak values found and the unit-cell dimensions (Table 1). This suggests that the higher initial pressure of 30 mN m^{-1} hinders the ability of the peptide to incorporate into the monolayer.

When the DPPG with PG-1 system was studied at 30 mN m^{-1} under constant area conditions, the calculated area per molecule of the condensed phase increased slightly after PG-1 insertion (Table 1, Fig. 2b). The data suggest that PG-1 inserts mostly into the disordered lipid phase, although some peptide molecules may adsorb underneath the solid domains due to charge interaction, giving rise to a dilated unit cell as observed with GIXD. The correlation length, L_{02}, decreased by almost 50% showing that there is an increased amount of peptide in the system.

XR – PG-1 at the air–aqueous interface

The surface activity of the PG-1 peptide was observed as there was an increase in pressure upon peptide injection while the

barriers were open, without any lipid film present. The jump of the surface pressure from 0 to 17 mN m^{-1} upon peptide introduction into the subphase clearly indicates that PG-1 is surface-active, even though the peptide is highly soluble in the aqueous subphase. The peptide surface layer is thus in equilibrium with the subphase, and the observed change in surface pressure is related to the amount of peptide adsorbed at the surface as given by the Gibbs adsorption equation.[24]

Analysis of the XR data (Fig. 3) suggests that when PG-1 was injected into the subphase, it adsorbed to and aligned at the air–aqueous interface, with its long axis oriented along the interface. Data of the pure PG-1 peptide film at the air–aqueous interface seem to further suggest the formation of two peptide layers at the air–aqueous interface, with the lower layer (L_2) being a partial layer due to the reduction in electron density in comparison to the upper layer, (L_1). These layers are most likely two layers of PG-1 due to their similar thicknesses that match closely with the cross-sectional diameter of the peptide from previous NMR studies.[15]

XR – interactions of PG-1 with lipid monolayers at 20 mN m^{-1}

Data for the DPPC system at 20 mN m^{-1} before and after injection of PG-1 into the subphase (Fig. 4a) suggest that there was some PG-1 insertion into the DPPC monolayer at 20 mN m^{-1} since the changes in the electron density are in accordance with a certain degree of PG-1 insertion, mainly into the head group region of the monolayer. Since there is a decrease in the area per lipid molecule whilst there is little disordering of the lipid monolayer, it could be suggested that the formation of peptide-rich and peptide-poor regions have been formed, such as we suggest occurs with lipid A monolayers (see below).

When analyzing the XR data of the lipid A with PG-1 system (Fig. 4b), the increase in electron density of L_1, along with the decrease in electron density of L_2, indicates that PG-1 molecules have fully inserted into the lipid A monolayer in some regions, with the majority of insertion occurring into the head group regions of the monolayer. However, one cannot discern from the data whether the peptide molecules are uniformly distributed between the lipid A molecules or they group together in between the lipid A molecules. It has been suggested that this grouping together of peptide molecules, which then align at the interface, may be more likely than the individual peptide molecules inserting randomly between lipid A molecules, as the lipid A molecules have bulky rigid tail group structures.[31]

XR – interactions of PG-1 with lipid monolayers at 30 mN m^{-1}

XR data of the DPPC with PG-1 system at 30 mN m^{-1} show that there is some degree of insertion due to an increase in the electron density of L_1 and a decrease in that of L_2. The DPPC at 30 mN m^{-1} with PG-1 data (Fig. 5a) suggest that there may be some compaction of lipid molecules due to peptide insertion under constant area conditions. This is in contrast to the GIXD data, which suggest little insertion. However, since GIXD is only sensitive to the ordered domains in the film, while XR takes into account both the ordered and the disordered regions, if the peptide were to insert only into the disordered region without disturbing the structure in the ordered region, we would expect to obtain XR results that indicate the incorporation of the peptide in the film and GIXD results that show little change from before peptide injection, both of which are observed here.

The XR data for the DPPG system at 30 mN m^{-1} (Fig. 5b) are best described by a two-layer model with thicknesses of 18.1 and 5.9 Å (Table 2). This is indicative of a DPPG phospholipid monolayer, with a tail group region and a head group region, respectively, as previously published.[8] After injection of PG-1, the data could no longer be modeled adequately with a two-layer model and a third layer was required. The data show that the tail layer reduces in thickness whilst the head group layer increases in thickness and decreases in electron density. The third layer has a thickness of 6.1 Å and a normalized electron density of 1.21. From the XR data for the DPPG system with PG-1 at 30 mN m^{-1}, it can be suggested that the PG-1 inserts into the DPPG head groups with the remaining part of the peptide protruding into the subphase, possibly giving rise to a partial peptide adsorbed layer. The fact that the tail group layer electron density does not change implies that the peptide does not fully penetrate through the DPPG monolayer. As a third layer was required to model the data adequately, the data suggest that the peptide is protruding out from the head group layer. This third layer is around one quarter of the thickness of the adsorbed layers, which occur at 20 mN m^{-1} (Table 2) suggesting that if peptide adsorption does occur at 30 mN m^{-1}, the peptides are aligned with the long axis parallel to the interface rather than perpendicular to it, as was proposed to occur at 20 mN m^{-1}.

The observation of an increase in area per molecule in the DPPG systems after PG-1 injection as compared to a decrease observed in equivalent DPPC systems suggests that the peptide interacts significantly differently with DPPG *versus* DPPC monolayers. These differences in interactions can only be due to differences in head group region, with DPPC being zwitterionic and DPPG anionic, since the tail groups of the lipid molecules are completely identical.[23]

Schematic cartoons

Complementary data from GIXD and XR allow us to speculate how the PG-1 peptide interacts with different lipid monolayers. The data analysis suggests that there is some low degree of interaction between PG-1 and DPPC monolayers, but its interaction is much more extensive with DPPG and lipid A monolayers. The data also show that PG-1 forms a surface active layer.

Our X-ray reflectivity results (Fig. 3) indicate that PG-1 aligns at the surface and that there is a partial second layer of PG-1 underneath the top layer. A schematic cartoon of the alignment of PG-1 molecules at the air–aqueous interface is shown in Fig. 6. It is possible to come up with this diagram as the approximate dimensions of the molecule are known[22,25] and the thicknesses of the layers are taken from the X-ray reflectivity fitting results.

When the GIXD and XR data for the DPPC with PG-1 system at 30 mN m^{-1} were further examined, it appeared that peptide

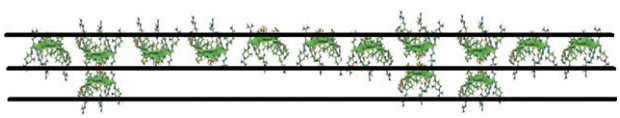

Fig. 6 Schematic cartoon of PG-1 film at the air–aqueous interface.

penetration into the DPPC monolayer was more limited in comparison to the DPPG and lipid A systems, and that the majority of the peptide insertion occurred into the head groups of the DPPC monolayer. Although GIXD data show little difference after PG-1 injection, XR data indicate that the PG-1 peptide does interact with the DPPC monolayer, most likely in the disordered region of the film. The schematic model proposed here in Fig. 7a is based on the fact that the head group layer decreases in electron density and increases in thickness as a result of peptide insertion. The tail group also increases in thickness and electron density, which we interpret as being due to the compaction of lipid molecules induced by peptide insertion.

Fig. 7b shows a schematic cartoon of the proposed mode of interaction of PG-1 with the DPPG monolayer at 30 mN m^{-1} based on results from the X-ray data. The DPPG monolayer has a tightly packed ordered structure at 30 mN m^{-1}, which is disturbed after PG-1 injection, as the peptide penetrates the DPPG monolayer. Some regions of ordered lipid structure may remain intact, but the overall structure of the DPPG monolayer is altered, with regions of peptide inserted into it, regions of peptide protruding from the head group layer of the monolayer, as well as a partial peptide adsorption to the underside of the DPPG monolayer.

In contrast, Fig. 7c shows a schematic of how PG-1 molecules may penetrate lipid A monolayers at 20 mN m^{-1}. The schematic is based on insertion assay data where an increase in pressure to 39 mN m^{-1} was observed. The model also takes into account GIXD and X-ray reflectivity data, which show that PG-1 peptides penetrate the lipid A monolayer and adsorb to it on the subphase side as shown by the third slab in the model.

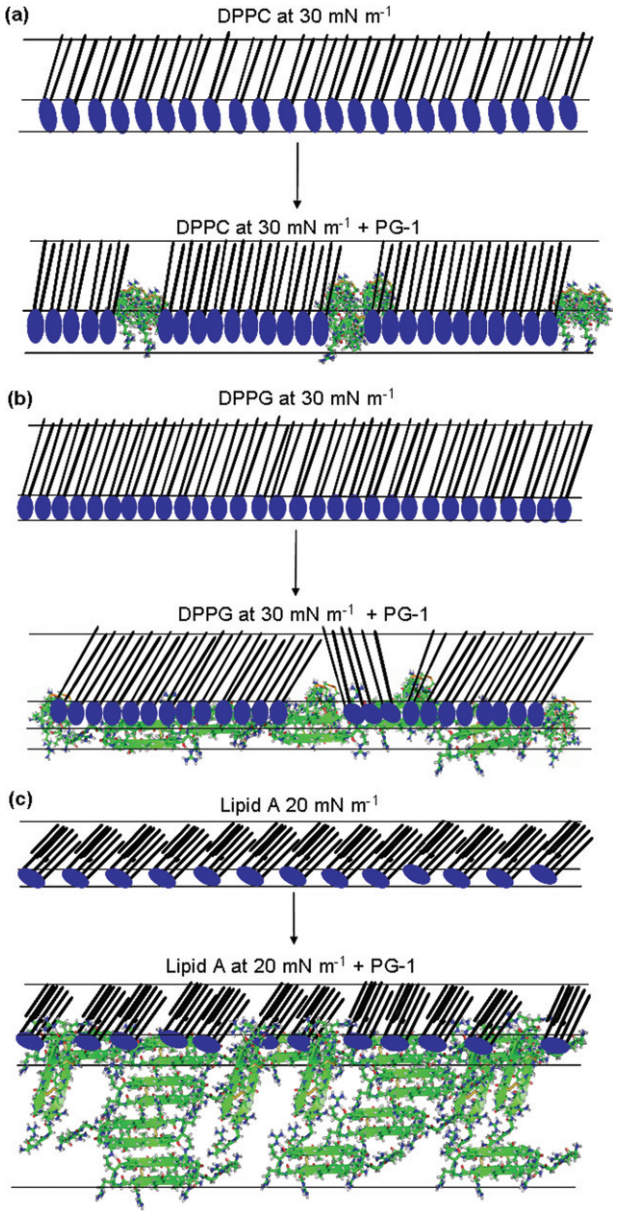

Fig. 7 Cartoon schematic of possible interactions of PG-1 with A) DPPC monolayer at 30 mN m^{-1}; B) DPPG monolayer at 30 mN m^{-1}; and C) lipid A monolayer at 20 mN m^{-1}.

Experimental

Lipid monolayers

The cell membranes of different organisms have characteristic lipid compositions. In order to study the targeting selectivity of PG-1, Langmuir monolayers composed of lipids representative of different membranes were examined. This approach has been utilized repeatedly over the years to elucidate peptide–membrane interactions.[26,27] In order to develop a full understanding of membrane interactions, each lipid component was studied separately in order to ascertain the contribution of each membrane component to the overall interaction of the peptide with the membrane. Dipalmitoyl phosphatidylcholine (DPPC), dipalmitoyl phosphatidylglycerol (DPPG) and lipid A were used to form Langmuir monolayers. In this work, DPPC was used as it is a major component of the outer leaflet of human red blood cell membranes.[10,28] DPPG is a representative lipid of the outer leaflet of the Gram-positive bacterial membrane[29,30] and lipid A is the lipid anchor of lipopolysaccharides from the outer membrane of Gram-negative bacteria. DPPC is zwitterionic, whereas DPPG and lipid A are negatively charged in solution. Lipids were prepared as described earlier.[8,22,31] DPPC and DPPG were purchased from Avanti Polar Lipids, and lipid A was purchased from Sigma-Aldrich. All lipids were used without further purification.

Peptides

Protegrin-1 (PG-1) (RGGRLCYCRRRFCVCVGR) is a porcine antimicrobial peptide.[15] The PG-1 peptide used in this study was synthesized in-house, and details of the synthesis have been published elsewhere.[15] The PG-1 solution was made up in 0.01% w/v acetic acid to a working solution with a concentration of 1 mg ml^{-1}. This, when injected into the subphase gave a final concentration of 0.025 mg ml^{-1}. The concentration of PG-1 used here was used in previous studies on *C. albicans*, *L. monocytogenes* and *E. coli* where it was shown to have potent microbicidal activity.[13] The concentration used is also known to be around the value of the minimum inhibitory concentration of several bacteria including *E. faecalis*, *P. aeruginosa*[14] and *L. interrogans.*[32]

Langmuir trough conditions

X-Ray scattering measurements were taken on the ID10B (Troika II) synchrotron beamline at the European Synchrotron Radiation Facility[33] and at the 9-ID (CMC-CAT) beamline at the Advance Photon Source, Argonne National Laboratory.[34] Both setups used PTFE (Teflon)-lined Langmuir troughs equipped with a single moveable barrier as described previously.[8,31,33]

Peptide-insertion technique

Upon spreading, the lipid film was left undisturbed for 15 minutes to allow for solvent evaporation. Subsequently, barrier compression (at 2 cm^2 min^{-1}) was initiated to attain the target surface pressure, which corresponds to the condensed phase of lipids (20–40 mN m^{-1}). These pressures were chosen so that the lipid packing density was equivalent to that of the cell membrane.[35] Moreover, the condensed phase condition also allowed us to monitor changes in lipid packing during PG-1 insertion. After reaching the target surface pressure, the insertion assay was then carried out in the constant area mode, where changes in the surface pressure indicate the degree of interaction of the peptide with the lipid monolayer. In this mode, the barrier motors were simply switched off whilst the peptide solution was uniformly injected underneath the monolayer with an L-shaped needle (VDRL needle; Hamilton, Reno, NV, USA). The introduction of peptides under the compressed lipid monolayer mimics the approach by the peptide to the outer surface of the cell, as the hydrophilic head groups are closest to the subphase, with the lipid film simulating the outer leaflet of the membrane and the peptide in the subphase mimicking the peptide in the extracellular fluid. Changes in pressure were recorded as a function of time during and after peptide injection into the subphase. All experiments were carried out using the constant area mode, and the surface pressure condition mentioned refers to the target surface pressure to which the monolayer was compressed at the start of the experiment.

Grazing incidence X-ray diffraction (GIXD) and X-ray reflectivity (XR)

Grazing incidence X-ray diffraction (GIXD)[27,36,38] was used to obtain in-plane information concerning the molecular structure of surfaces, whereas specular XR measurements[27,36,38] revealed information on the electron density distribution along the surface normal and may be used to determine the density and thickness of thin layers.[27,36,38]

X-Ray scattering measurements were carried out at the ID10B (Troïka II) beamline at the European Synchrotron Radiation Facility, France, as previously described, and data were analyzed as before.[8,31,33] Control measurements of pure lipid monolayers were followed by subsequent injection of the desired amount of peptide into the subphase under a monolayer compressed to the desired surface pressure.

Grazing incidence X-ray diffraction measurements were made with variation of the X-ray momentum transfer component q_{xy} that is parallel to the air–aqueous interface. The reflections of the Bragg peaks observed with this geometry can be indexed by two Miller indices, hk. Their angular position $2\theta_{hk}$, corresponding to $q_{hk} = (4\pi/\lambda)\ \sin\ \theta_{hk}$, yields the repeat distance $d_{hk} = 2\pi/q_{hk}$ for the two-dimensional (2D) lattice structure.[39,40] Bragg peak profiles (intensity against q_{xy}) were fitted with Gaussians and the peak position values were used to obtain unit-cell dimensions of the lipid lattices. The observation of two Bragg peaks in the diffraction pattern of an amphiphilic monolayer is indicative of a distorted hexagonal unit cell (which may be better described[39] as a centered rectangular unit cell). Therefore, all unit-cell dimensions in this paper have been calculated using the centered rectangular unit cell approximation. Full-width at half-maximum (FWHM) values of the Bragg peaks were used to determine the correlation length from the Scherrer formula,[8,40,41] $L = \sim 0.9(2\pi/\mathrm{FWHM}_{(q_{xy})})$, where $\mathrm{FWHM}_{(q_{xy})}$ is the resolution corrected full-width at half-maximum in q_{xy} units ($Å^{-1}$). The correlation length is a length restriction caused by inhomogeneities in the sample and a reduction in the correlation length is indicative that the monolayer has more impurities or it is made of two components, such as the monolayer and peptide inserting in to the monolayer.

As well as Bragg peak profiles, Bragg rod profile measurements[27,37] were also taken during GIXD measurements. From the Bragg rod profiles it is possible to determine if the molecules are tilted and to calculate the tilt angle of the molecules at the air–aqueous interface, using the maximum values of the Bragg rod profiles (see ESI†), which plot the intensity against q_z.[27,37] In simple terms, when $q_z \neq 0$, tilt $(t) = q_{z,11}(2\pi/a)$, where $q_{z,11}$ is the peak value of the $\{11\}^a q_z$ peak and a is the unit cell dimension calculated from Bragg peak values.[37] The tilt angle can be used to determine if the relevant layer thickness value, L, obtained with the XR fitting is appropriate (see ESI†) using $L = \cos(t)L_{\max}$, where $L_{\max}$ is the maximal tail length given by $1.5 + n1.265$ Å.[42]

XR is measured as a function of the scattering vector q_z, where $q_z = 2\pi/\lambda\ (\sin\ \alpha)$, α is the grazing angle of the incident beam and λ the wavelength of the X-ray beam. The reflectivity curve contains information regarding the gradient of the electron density profile in the direction normal to the surface.[8,39] X-Ray reflectivity measurements were carried out at a range of angles corresponding to q_z values of approximately 0 to 0.65 $Å^{-1}$. The reflected beam intensity was measured as a function of the incident angle using a position sensitive detector.

The XR data were then analyzed using data processing and fitting programs as carried out previously[8,31,33] in order to gain information on the electron density distribution in the direction normal to the surface. This provided an electron density profile averaged laterally over both ordered and disordered parts of the system. The whole monolayer and subphase system was modelled as slabs, or layers, where each slab has a constant electron density and thickness.[33]

Conclusions

In conclusion, the work presented here consolidates and reinforces earlier work carried out using epifluorescence microscopy and X-ray scattering methods,[22,23] and thoroughly investigates the interaction of PG-1 with different lipids using X-ray scattering techniques. From the changes in ordering, area per molecule and unit-cell dimensions, GIXD data show that PG-1 interacts with and inserts into DPPC monolayers. However, unlike the case of DPPG, under none of the conditions examined

does PG-1 injection result in the complete disordering of DPPC packing, suggesting that electrostatic forces are playing an important role in the interaction. Our data further show that while PG-1 inserts into DPPC, DPPG and lipid A monolayers under constant area conditions and primarily into the head group region, the effect of the peptide on the DPPG and lipid A monolayers is much more pronounced than that on the DPPC monolayer, and an additional peptide adsorbed layer was only observed below the head group region for the two anionic lipid systems. Our data further suggest that there is a much greater extent of disordering in lipid systems with lower packing due to PG 1 insertion, in agreement with our earlier findings from epifluorescence microscopy.[22,23] The fact that PG-1 preferentially damages lipid monolayers composed of lipids prevalent in different types of bacteria suggests that PG-1 is a good candidate for antimicrobial drug targets to be designed in the future. This bodes well for the design and development of protegrins and other antimicrobial peptides as future therapeutic agents.

Acknowledgements

We acknowledge the European Synchrotron Radiation Facility for provision of synchrotron radiation facilities at the ID10B beamline. Use of the Advanced Photon Source was supported by the U.S. Department of Energy, Office of Science, Office of Basic Energy Sciences, under Contract no. W-31-109-ENG-38. YI and KYCL are grateful for the support of the Packard Foundation (99-1465). FN and DG would like to acknowledge the sponsorship of this work by the Engineering and Physical Sciences Research Council, UK.

References

1 M. Zasloff, *N. Engl. J. Med.*, 2002, **347**, 1199–1200; R. Bals and J. M. Wilson, *Cell. Mol. Life Sci.*, 2003, **60**, 711–720.
2 D. A. Devine and R. E. W. Hancock, in *Mammalian Host Defense Peptides*, Cambridge University Press, Cambridge, 1st edn, 2004, vol. 6; D. Yang, A. Biragyn, D. M. Hoover, J. Lubkowski and J. J. Oppenheim, *Annu. Rev. Immunol.*, 2004, **22**, 181–215; D. M. E. Bowdish, D. J. Davidson, M. G. Scott and R. E. W. Hancock, *Antimicrob. Agents Chemother.*, 2005, **49**, 1727–1732.
3 Z. Oren and Y. Shai, *Biopolymers*, 1998, **47**, 451–463; Y. Shai, *Biochim. Biophys. Acta: Biomembranes*, 1999, **1462**, 55–70.
4 K. Matsuzaki, *Biochim. Biophys. Acta*, 1999, **1462**, 1–10.
5 B. Pozo Navas, K. Lohner, G. Deutsch, E. Sevcsik, K. A. Riske, R. Dimova, P. Garidel and G. Pabst, *Biochim. Biophys. Acta*, 2005, **1716**, 40–48.
6 K. Lohner and E. J. Prenner, *Biochim. Biophys. Acta*, 1999, **1462**, 141–156.
7 F. Neville, M. Cahuzac, A. Nelson and D. Gidalevitz, *J. Phys.: Condens. Matter*, 2004, **16**, S2413–S2420.
8 F. Neville, M. Cahuzac, O. Konovalov, Y. Ishitsuka, K. Y. C. Lee, I. Kuzmenko, G. M. Kale and D. Gidalevitz, *Biophys. J.*, 2006, **90**, 1275–1287.
9 J. M. Graham, in *Membrane Analysis*, ed. J. M. Graham and J. A. Higgins, Springer, New York, 1997.
10 S. L. Keller, W. H. Pitcher, W. H. Huestis and H. M. McConnell, *Phys. Rev. Lett.*, 1998, **81**, 5019–5022.
11 C. Ratledge and S. G. Wilkinson, in *Microbial Lipids*, Academic Press, London, 1988.
12 A. J. Burton and H. E. Carter, *Biochemistry*, 1964, **3**, 411–418; K. Takayama, N. Qureshi, P. Mascagni, M. Nashed, L. Anderson and C. Raetz, *J. Biol. Chem.*, 1983, **258**, 7379–7385.
13 V. N. Kokryakov, S. S. L. Harwig, E. A. Panyutich, A. A. Shevchenko, G. M. Aleshina, O. V. Shamova, H. A. Korneva and R. I. Lehrer, *FEBS Lett.*, 1993, **327**, 231–236.
14 D. Steinberg, M. Hurst, C. Fujii, A. Kung, J. Ho, F. Cheng, D. Loury and J. Fiddes, *Antimicrob. Agents Chemother.*, 1997, **41**, 1738–1742.
15 R. L. Fahrner, T. Dieckmann, S. S. L. Harwig, R. I. Lehrer, D. Eisenberg and J. Feigon, *Chem. Biol.*, 1996, **3**, 543–550.
16 H. Tamamura, T. Murakami, S. Horiuchi, K. Sugihara, A. Otaka, W. Takada, T. Ibuka, M. Waki, N. Yamamoto and N. Fujii, *Chem. Pharm. Bull.*, 1995, **43**, 853–858.
17 B. Yasin, S. S. Harwig, R. I. Lehrer and E. A. Wagar, *Infect. Immunol.*, 1996, **64**, 709–713.
18 W. T. Heller, A. J. Waring, R. I. Lehrer and H. W. Huang, *Biochemistry*, 1998, **37**, 17331–17338.
19 C. Ma, M. P. Srinivasan, A. J. Waring, R. I. Lehrer, M. L. Longo and P. Stroeve, *Colloids Surf., B*, 2003, **28**, 319–329.
20 R. Mani, M. Tang, X. Wu, J. J. Buffy, A. J. Waring, M. A. Sherman and M. Hong, *Biochemistry*, 2006, **45**, 8341–8349.
21 R. Mani, S. D. Cady, M. Tang, A. J. Waring, R. I. Lehrer and M. Hong, *Proc. Natl. Acad. Sci. U. S. A.*, 2006, **103**, 16242–16247.
22 D. Gidalevitz, Y. J. Ishitsuka, A. S. Muresan, O. Konovalov, A. J. Waring, R. I. Lehrer and K. Y. C. Lee, *Proc. Natl. Acad. Sci. U. S. A.*, 2003, **100**, 6302–6307.
23 Y. Ishitsuka, D. S. Pham, A. J. Waring, R. I. Lehrer and K. Y. C. Lee, *Biochim. Biophys. Acta*, 2006, **1758**, 1450.
24 J. R. Lu, R. K. Thomas and J. Penfold, *Adv. Colloid Interface Sci.*, 2000, **84**, 143–304; M. Yaseen, Y. Wang, T. J. Su and J. R. Lu, *J. Colloid Interface Sci.*, 2005, **288**, 361–370.
25 L. Zhang, R. Vidu, A. J. Waring, R. I. Lehrer, M. L. Longo and P. Stroeve, *Langmuir*, 2002, **18**, 1318–1331.
26 R. Maget-Dana, *Biochim. Biophys. Acta*, 1999, **1462**, 109–140; H. Brockman, *Curr. Opin. Struct. Biol.*, 1999, **9**, 438–443; S. Castano, B. Desbat and J. Dufourcq, *Biochim. Biophys. Acta*, 2000, **1463**, 65–80; M. Lösche, in *Current Topics in Membranes*, ed. S. A. Simon and T. J. McIntosh, Academic Press, New York, 2002, pp. 117–161; F. Sun, *Biophys. J.*, 2002, **82**, 2511–2519; E. E. Ambroggio, F. Separovic, J. Bowie and G. D. Fidelio, *Biochim. Biophys. Acta*, 2004, **1664**, 31–37.
27 T. R. Jensen, K. Balashev, T. Bjornholm and K. Kjaer, *Biochimie*, 2001, **83**, 399–408.
28 M. H. Nouri-Sorkhabi, L. C. Wright, D. R. Sullivan and P. W. Kuchel, *Lipids*, 1996, **31**, 765–770.
29 H. Goldfine, *Adv. Microb. Physiol.*, 1972, **8**, 1–58; J. A. F. Op den Kamp, *Annu. Rev. Biochem.*, 1979, **48**, 47–71.
30 G. Basañez, A. E. Shinnar and J. Zimmerberg, *FEBS Lett.*, 2002, **532**, 115–120.
31 F. Neville, C. S. Hodges, C. Liu, O. Konovalov and D. Gidalevitz, *Biochim. Biophys. Acta*, 2006, **1758**, 232–240.
32 V. Sambri, A. Marangoni, L. Giacani, R. Gennaro, R. Murgia, R. Cevenini and M. Cinco, *J. Antimicrob. Chemother.*, 2002, **50**, 895–902.
33 O. Konovalov, I. Myagkov, B. Struth and K. Lohner, *Eur. Biophys. J. Biophys. Lett.*, 2002, **31**, 428–437.
34 W.-J. Pao, F. Zhang, P. A. Heiney, C. Mitchell, W.-D. Cho and V. Percec, *Phys. Rev. E*, 2003, **67**, 021601.
35 R. A. Demel, W. S. M. Geurts van Kessel, R. F. A. Zwaal, B. Roelofsen and L. L. M. van Deenen, *Biochim. Biophys. Acta*, 1975, **406**, 97–107; A. Blume, *Biochim. Biophys. Acta*, 1979, **557**, 32–44.
36 J. Als-Nielsen and D. McMorrow, in *Elements of Modern X-Ray Physics*, John Wiley & Sons, Chichester, 1st edn, 2001.
37 T. R. Jensen and K. Kjaer, in *Novel Methods to Study Interfacial Layers*, ed. D. Möbius and R. Miller, Elsevier, Amsterdam, 2001, pp. 205–254.
38 M. Schalke and M. Lösche, *Adv. Colloid Interface Sci.*, 2000, **88**, 243–274.
39 J. Als-Nielsen, D. Jacquemain, K. Kjaer, F. Leveiller, M. Lahav and L. Leiserowitz, *Phys. Rep.*, 1994, **246**, 251–313.
40 F. Leveiller, D. Jacquemain, L. Leiserowitz, K. Kjaer and J. Als-Nielsen, *J. Phys. Chem.*, 1992, **96**, 10380–10389.
41 R. Stömmer and U. Pietsch, *J. Phys. D: Appl. Phys.*, 1996, **29**, 3161–3165; C. Ege, J. Majewski, M. Ratajczak, K. Kjaer and K. Y. C. Lee, *Biophys. J.*, 2006, **91**, L01–03.
42 C. A. Helm, H. Möhwald, K. Kjaer and J. Als-Nielsen, *Europhys. Lett.*, 1987, **4**, 697–703.

